Metamagnetism of $CoCl_3[(CH_3)_3NH]\cdot 2H_2O$

R. D. Spence
Department of Physics, Michigan State University, East Lansing, Michigan 48824

A. C. Botterman
Department of Physics, Eindhoven University of Technology, Eindhoven, The Netherlands

(Received 15 November 1973)

If a field $H > 64$ Oe is applied along the c axis of $CoCl_3[(CH_3)_3NH]\cdot 2H_2O$, the proton and chlorine NMR frequencies exhibit anomalous behavior which may be explained by a metamagnetic model in which all spins in certain bc planes reverse their directions. By minimizing the expressions for the energy of such a system, we derive the internal fields that arise from such a metamagnetic transition. It is shown that such internal fields yield the observed form of the field and angle dependence of the NMR frequencies. The observed angle dependence of the magnetization is also obtained from this model.

I. INTRODUCTION

According to the recent work of Losee *et al.*[1] the structure of $CoCl_3[(CH_3)_3NH]\cdot 2H_2O$ consists of planes of parallel $CoCl_3\cdot 2H_2O$ chains interleaved with planes of $(CH_3)_3NH$ groups. From heat-capacity and susceptibility studies, the same authors concluded that the compound orders as a canted antiferromagnet at (4.135 ± 0.006) °K. The combination of crystal structure, the a axis canting of spins, and an inferred ferromagnetic exchange along the b axis, also enabled these authors to propose a spin arrangement for the magnetically ordered state. When we attempted to check their proposed spin arrangement with NMR, we found that the application of a magnetic field whose projection on the c axis was greater than 64 Oe drastically modified the state of magnetization of the crystal. It now appears that these changes are associated with fact that the crystal shows metamagnetic behavior. The major portions of this paper (Secs. IV, V, and VI) deal with the experimental and theoretical aspects of the observed metamagnetism. However, in Sec. III we briefly outline the results of NMR observations at fields *less than* 64 Oe. The spin arrangement inferred from such experiments agrees with that given in Ref. 1. In addition, the discussion of compatible magnetic space groups contained in Sec. III furnishes a basis for the metamagnetic configurations used in the subsequent sections.

II. EXPERIMENTAL

The crystals used in these experiments were grown from an aqueous solution of cobalt chloride and trimethylamine hydrochloride. The specimens used in the NMR experiment had a length of ~1.0 cm along the b axis and ~0.3 cm along the perpendicular a and c axes. The crystal used in the magnetization experiments had dimensions $a = 0.2$ cm, $b = 0.35$ cm and $c = 0.3$ cm. The crystals exhibited an essentially invariant morphology, but despite this we checked the orientation of all specimens with x rays. The NMR signals were detected by the free-induction-decay technique or by a marginal oscillator. The latter proved somewhat superior in making measurements of frequencies of the observed lines. The magnetization was measured with a Faraday balance.

III. MAGNETIC SPACE GROUP

The structure[1] of $CoCl_3[(CH_3)_3NH]\cdot 2H_2O$ is shown in Fig. 1. The chemical space group is *Pnma* and its symmetry operations are given on the right-

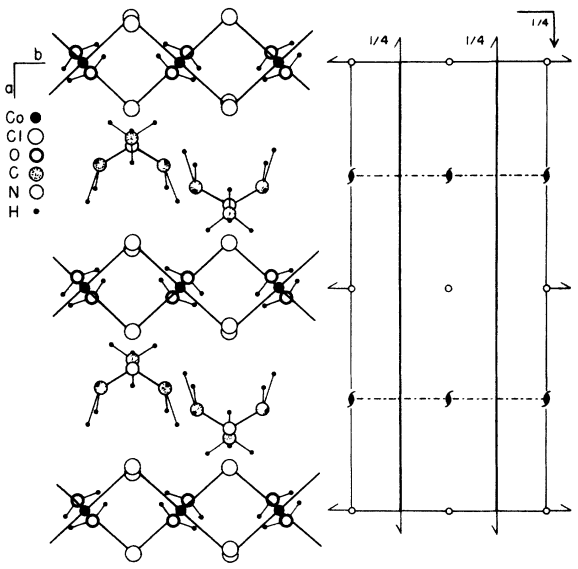

FIG. 1. Structure of $CoCl_3[(CH_3)_3NH]\cdot 2H_2O$ projected on the ab plane. The right-hand portion of the figure shows the crystallographic symmetry operations.

TABLE I. The family of magnetic space groups belonging to *Pnma*.

Group	$\bar{1}'$ absent	m' present	possible
Pnma	yes	no	no
Pn'ma	no	no	no
Pnm'a	no	yes	no
Pnma'	no	no	no
Pn'm'a	yes	yes	yes
Pnm'a'	yes	yes	yes
Pn'ma'	yes	no	no
Pn'm'a'	no	yes	no

hand side of Fig. 1. If there are no crystallographic changes between room temperature and the Néel temperature the magnetic space group should be a member of the family[2] of *Pnma*. The family of magnetic space groups belonging to *Pnma* are listed in the first column of Table I. Primes indicate anti-elements. Antitranslations which produce magnetic cells that are multiples of the chemical cell are forbidden in the family of *Pnma* by the presence of the *a* axis glide plane and the *b*- and *c*-axes screw axes. Thus all the possible space groups are based on the chemical unit cell. This is consistent with experimental observation that in the magnetically ordered state the system exhibits a moment along the $\pm a$ axis. Such a moment can occur only in magnetic space groups based on the chemical unit cell.

In the seven new magnetic space groups derived from *Pnma*, the inversion centers which occur in *Pnma* either remain inversion centers ($\bar{1}$) or become anti-inversion centers ($\bar{1}'$). Since the Co ions are located at inversion centers in *Pnma*, and since no magnetic moment can exist at an anti-inversion center, the four groups having anticenters can immediately be eliminated. These groups are marked with "no" in the second column of Table I.

We next consider the mirror plane of *Pnma*. In the magnetic structure this plane may either remain a mirror plane (m) or become an antimirror plane (m'). The mirror planes in question are shown as the heavy vertical lines in Fig. 1. All the chlorine ions and the one hydrogen from the NH group lie in these planes. Since the local magnetic field is an *axial* vector, it follows that at sites in the plane the local magnetic field will be parallel to the plane if the plane is of the m' type. Thus to determine whether the planes are of the m or m' type, one has only to find the direction of the local field at any one of the four varieties of nuclei in the plane. Table II shows the frequencies of the Cl^{35} lines belonging to the chlorine ions which form the bridge between Co ions. The central lines of each group are presumed to be the

TABLE II. Cl^{35} zero-field resonances[a] (in MHz) at 2.25 °K.

17.021	15.277
11.036	10.075
5.380	5.204

[a]Chlorines in Co-Cl-Co bridges only. Spectrum of nonbridging chlorine has not been identified.

$\frac{1}{2} \leftrightarrow -\frac{1}{2}$ transitions. Figure 2 shows the angle dependence of the splitting of these lines produced by a field of 50 Oe applied in the *ac* plane. The splitting reaches a maximum when the external field is along the *c* axis, and to within experimental error it corresponds numerically to the value expected for a situation in which the external and local magnetic fields are parallel. The mirror plane is therefore an antimirror plane m'. The magnetic moments at the Co sites in the chain along the *b* axis are all related by the same m' planes. The ferromagnetic exchange along the *b* axis allowed by this result is consistent with the conclusions of Losee *et al.*[1] In Table I we have indicated groups lacking the required m' plane by "no" in the third column. In the fourth column we see that only two groups, *Pn'm'a* and *Pnm'a'* satisfy both the condi-

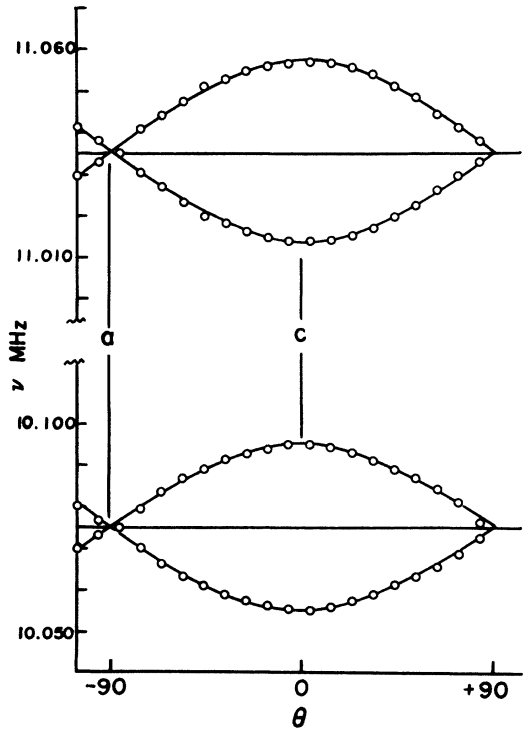

FIG. 2. Splitting of central lines of the Cl^{35} spectra in a field of 50 Oe applied in the *ac* plane.

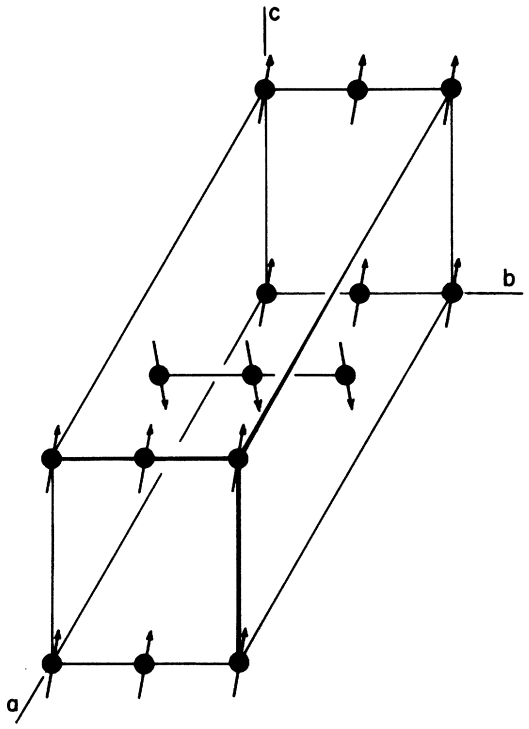

FIG. 3. Spin arrangement for $Pnm'a'$.

tions of the absence of $\bar{1}'$ and the presence of m'. Both of these groups permit the sample to exhibit a net moment. If the group is $Pnm'a'$, and if there is any component of the sublattice magnetization along the a axis, then the sample is required to exhibit a net moment along this axis. Alternatively if the group is $Pn'm'a$, and if there is any component of sublattice magnetization along the c axis, then the sample must exhibit a net moment along the c axis. The susceptibility results given in Ref. 1 indicate that the sublattice magnetization is nearly along the c axis. From NMR we find that for the chlorines bonded to the Co ions and the *protons in the waters of hydration* the local fields are very close to parallel to the c axis. Since the local fields at these sites (see Fig. 1) are determined primarily by the nearest Co ions our NMR results are in agreement with the sublattice magnetization direction given by Losee *et al.*[1] However, if the sublattice magnetization has any component along c, the group $Pn'm'a$ requires that a net moment exist in this direction. Since no indication of such a moment is observed for applied fields less than 64 Oe, one may reject the group $Pn'm'a$. The remaining possible group, $Pnm'a'$, permits a net moment parallel to the a axis. Experimentally the presence of even a minute field along the a axis is found to produce an appreciable magnetization in this direction. Thus it appears that although the Co spins are nearly parallel to the c axis, they are slightly canted towards the a axis. Such a configuration is permitted in the one surviving group, $Pnm'a'$. The spin arrangement implied by these observations is shown in Fig. 3. As a further check on the validity of the group $Pnm'a'$, we have measured the resonance frequencies of all the protons in zero applied field and compared them with frequencies computed from a model in which the Co ions are replaced with point dipoles whose orientation is consistent with this group. Figure 4 shows the results of such a comparison for a model in which the dipoles were oriented along the $\pm c$ axis and given moment $\mu_B gS$ with $S=\frac{1}{2}$ and $g=6.42$. The agreement is quite satisfactory, considering the crudeness of the model. The g value found in this way may be compared with the value of $g_c = 6.54 \pm 0.1$ given by Losee *et al.*[1] The relative success of our model with dipoles oriented only along the $\pm c$ axis does not imply that spin canting along the $\pm a$ axis does not exist. Using $g_a = 2.95$ given in Ref. 1 we find that a canting of less than $\simeq 15°$ does not materially degrade (or improve) the agreement indicated by Fig. 4. In a later section we shall show that the magnetization data allow one to estimate the canting angle as approximately 9.8°.

The zero-field proton frequencies given in Fig. 4 were measured at 2.25 °K. These frequencies vary less than 1% in the range from 1.1–3.0 °K. However, the intensity of the resonances decreases rapidly for $T > 2.5$ °K. This is apparently corre-

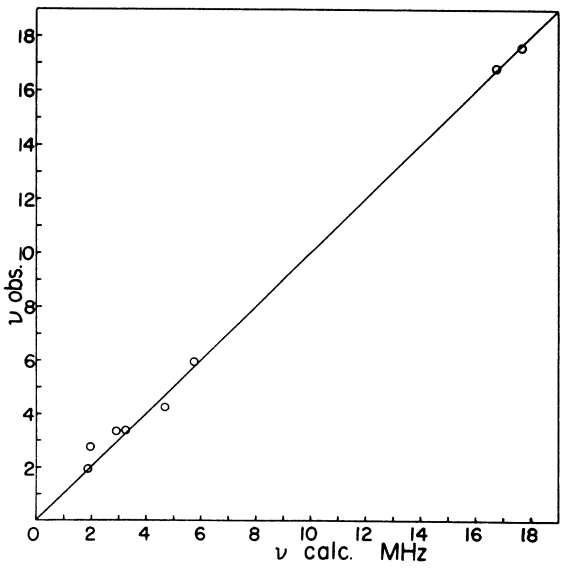

FIG. 4. Comparison of calculated and observed zero field proton resonance frequencies. Calculations based on $Pnm'a'$ and $g_c = 6.42$.

lated with the fact that the zero-field susceptibility[1] indicates that the magnetic structure is not well established[3] for $T > 2.5$ °K. Consequently in the remainder of the present paper the measurements and the models used to explain them are restricted to temperatures less than 2.5 °K.

IV. BEHAVIOR IN APPLIED FIELDS–METAMAGNETISM

In the following section we consider a model intended to explain the magnetic behavior of $CoCl_3[(CH_3)_3NH]\cdot 2H_2O$ in applied fields whose projection on the c axis may exceed 64 Oe. For the purpose of this and succeeding sections it is convenient to designate the components of magnetization along the crystallographic a and c axes with M_x and M_z. The symbols M_a and M_c will be reserved to designate the *saturation* values of the corresponding components.

In Sec. III it was noted that the magnetic space group $Pnm'a'$, which described the magnetic properties of the crystal for applied fields less than 64 Oe, permits net magnetic moment along the $\pm x$ directions. If the applied field along $\pm x$ is *strictly* zero the $\pm x$ directions are physically indistinguishable and, as might be expected, no magnetization is observed in this direction. Since even a minute field along $\pm x$ leads to a very sizable magnetization in this direction, we conclude that the zero-field situation must be described by equal volumes of the crystal having opposite directions of magnetization. This agrees with the experimental observation that the susceptibility parallel to the a axis is quite small for $T < 2.5$ °K. In addition, if a field having a component along the z axis of greater than 64 Oe is applied, a large magnetization develops in this direction. Such a magnetization corresponds to the magnetic space group $Pn'm'a$, which we previously eliminated as representing the zero-field situation. Clearly we deal here with a situation in which the energy of a spin configuration described by $Pn'm'a$ lies only slightly above the configuration described by $Pnm'a'$. Using the value $H_k = 64$ Oe at which magnetization appears along the z axis we estimate this energy difference as

$$\Delta E \simeq g_c \mu_B H_k / 2k = 1.4\times 10^{-3}\ ^\circ\mathrm{K}\ .$$

Presumably this energy is that required to reverse the moments in one of the ferromagnetic bc planes shown in Fig. 3 and thereby generate a region in which the magnetic symmetry in $Pn'm'a$ rather than $Pnm'a$. The smallness of the energy involved must indicate that the antiferromagnetic coupling through the layers of $(CH_3)_3NH$ groups between the ferromagnetic bc planes is very weak.

To compute[4] the magnetization which is to be expected when a field of arbitrary magnitude and orientation is applied, we assume that the sample consists of regions in which the spin orientations correspond to any one of the configurations C_1, C_2, C_3 shown in Fig. 5. C_1 and C_3 correspond to $Pnm'a'$ and C_2 corresponds to $Pn'm'a$. Let f_1, f_2, f_3 be the fractions of the total sample volume occupied by each of the corresponding spin configurations. Then

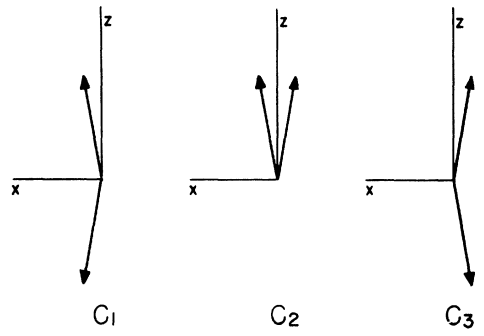

FIG. 5. The spin configurations C_1, C_2, and C_3. C_1 and C_3 correspond to the group $Pnm'a'$ and C_2 corresponds to $Pn'm'a$.

$$f_1 + f_2 + f_3 = 1 = M_x/M_a + M_z/M_c + 2f_3\ . \tag{1}$$

The magnetic energy consists of the usual magnetostatic term plus the energy to create the configuration C_2 from the configurations C_1 and C_3. The latter energy is proportional to the volume of f_2 and hence to the magnetization M_z. Thus the magnetic energy per unit volume may be written,

$$\mathcal{E}_m = -\int \vec{H}_i \cdot d\vec{M} + H_k \int dM_z\ , \tag{2}$$

where $\vec{H}_i$ is the internal field arising from the combined effects of the applied field $\vec{H}$ and the consequent sample magnetization $\vec{M}$. H_k appears as a proportionality constant which we recognize as the critical field $H_k = 64$ Oe. When minimizing $\mathcal{E}_m$ subject to the restriction of Eq. (1) one notes there are two distinct possibilities to be considered: (A) $f_3 \neq 0$; (B) $f_3 = 0$. In region A, M_x and M_z are independent and hence

$$H_{ix} = 0\ , \tag{3a}$$

$$H_{iz} - H_k = 0\ . \tag{3b}$$

For region B the components of magnetization are related by

$$M_x/M_a + M_z/M_c = 1\ , \tag{4}$$

and hence

$$H_{ix}M_a - (H_{iz} - H_k)M_c = 0\ . \tag{5}$$

To calculate the magnetization of either region A or B, one needs a relation connecting the internal field $\vec{H}_i$, the applied field $\vec{H}$ and the magnetization

$\vec{M}$. The simplest possibility is the linear relation

$$\vec{H}_i = \vec{H} - \vec{\vec{N}}\cdot\vec{M} . \tag{6}$$

There is some doubt as to whether the tensor $\vec{\vec{N}}$ can be considered to be an ordinary demagnetization tensor. Even though the sample shape can be made ellipsoidal, the model we have assumed, allows the magnetization to be spatially inhomogeneous. Despite this objection it appears that the linear relation of Eq. (6) is capable of explaining our experimental results.

The magnetization has only components along x and z axes. We assume that these axes also diagonalize $\vec{\vec{N}}$ and write the corresponding elements as N_{xx} and N_{zz}. The expressions for the components of magnetization are simplified if we introduce the abbreviations

$$H_a = N_{xx}M_a , \tag{7a}$$

$$H_c = N_{zz}M_c , \tag{7b}$$

$$\rho = H_a/H_c , \tag{7c}$$

$$r = M_a/M_c . \tag{7d}$$

Let θ represent the angle between the z axis and the applied field $\vec{H}$. One finds for the components of $\vec{M}$

region A $(M_x/M_a + M_z/M_c < 1)$

$$M_x = N_{xx}^{-1}H\sin\theta , \tag{8a}$$

$$M_z = N_{zz}^{-1}(H\cos\theta - H_k); \tag{8b}$$

region B $(M_x/M_a + M_z/M_c = 1)$

$$M_x = N_{xx}^{-1}(1+r\rho)^{-1}[r\rho H\sin\theta - \rho(H\cos\theta - H_k - H_c)], \tag{9a}$$

$$M_z = N_{zz}^{-1}(1+r\rho)^{-1}[(H\cos\theta - H_k) - r(H\sin\theta - H_a)] . \tag{9b}$$

The expressions for M_x and M_z in Eqs. (8a) and (8b) become identical with those of Eqs. (9a) and (9b) along the curve

$$H\sin\theta - H_a + \rho(H\cos\theta - H_k) = 0 . \tag{10}$$

Two important subcases of Eq. (4) are the following:

region α (M_z *saturated*)

$$M_x = 0, \tag{11a}$$

$$M_z = M_c . \tag{11b}$$

This joins region B along the curve

$$H\cos\theta - H_c - H_k - rH\sin\theta = 0 . \tag{12}$$

Region β (M_x *saturated*)

$$M_x = M_a , \tag{13a}$$

$$M_z = 0 . \tag{13b}$$

This joins region B along the curve

$$H\cos\theta - H_k - r(H\sin\theta - H_a) = 0 . \tag{14}$$

One further case must be considered. If $H_z < H_k$ and $H_x \neq 0$, then $f_2 = 0$ and we have

region γ:

$$M_x = N_{xx}^{-1}H\sin\theta , \tag{15a}$$

$$M_z = 0 . \tag{15b}$$

The boundary curve for this region is

$$H\cos\theta - H_k = 0 . \tag{16}$$

In the $H\theta$ plane the different functional forms for the components of magnetization which we have designated by A, B, α, β, γ occur in five different regions as shown in Fig. 6. The components of the internal field $\vec{H}_i$ in each of the five different regions may be found by inserting the appropriate components of magnetization in Eq. (6). We summarize the results:

region A

$$H_{ix} = 0, \tag{17a}$$

$$H_{iz} = H_k ; \tag{17b}$$

region B

$$H_{ix} = (1+r\rho)^{-1}[H(\rho\cos\theta + \sin\theta) - \rho(H_k + H_c)], \tag{18a}$$

$$H_{iz} = (1+r\rho)^{-1}[rH(\rho\cos\theta + \sin\theta) + (H_k - rH_a)]; \tag{18b}$$

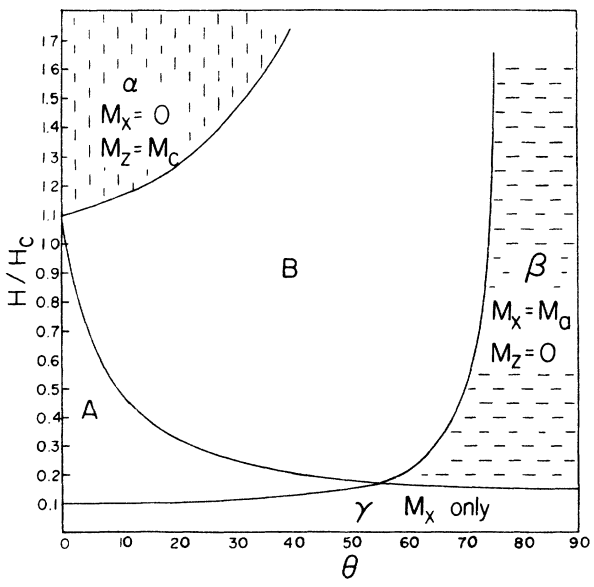

FIG. 6. Regions of magnetization in the $H\theta$ plane.

TABLE III. Local fields H_l for water protons in C_1+C_3 material.

Site	Magnitude[a] (kOe)	ϑ, angle from $+z$ axis
1, 2	4.136	−14.4°
3, 4	4.136	−165.6°
5, 6	3.953	+13.0°
7, 8	3.953	+167.0°

[a]At 2.25°K.

region α

$$H_{ix} = H\sin\theta\,, \tag{19a}$$

$$H_{iz} = H\cos\theta - H_c\,; \tag{19b}$$

region β

$$H_{ix} = H\sin\theta - H_a\,, \tag{20a}$$

$$H_{iz} = H\cos\theta\,; \tag{20b}$$

region γ

$$H_{ix} = 0\,, \tag{21a}$$

$$H_{iz} = H\cos\theta\,. \tag{21b}$$

In the following sections we compare the experimental NMR and magnetization results with the predictions based on the previous expressions for the components of $\vec{H}_i$ and $\vec{M}$.

V. FIELD AND ANGLE DEPENDENCE OF THE NMR LINES

In this section we show that the expressions for the internal field $\vec{H}_i$ given in Sec. IV yield a correct description of the NMR results in an applied field $\vec{H}$. The *total* field at a nuclear site is the sum of the internal field $\vec{H}_i$ and the local field $\vec{H}_l$. For protons the resonance frequency ν is given in terms of $\vec{H}_i$ and $\vec{H}_l$ by the simple relation,

$$\nu = \gamma_p\left|\vec{H}_l + \vec{H}_i\right|\,, \tag{22}$$

provided the nuclear dipole-dipole interaction is negligible. For the chlorine nuclei $I=\frac{3}{2}$ and the spectrum arises from three transitions. The three transitions are distinct because the Cl Hamiltonian contains a quadrupole term in addition to the Zeeman term from the field $\vec{H}_l+\vec{H}_i$. The only problem connected with expressing the NMR results in terms of $\vec{H}_i$ is in determining the local field $\vec{H}_l$. Since $\vec{H}_i$ vanishes if the applied field $\vec{H}$ is zero, it might appear that $\vec{H}_l$ could be determined from resonance experiments done with $\vec{H}$ zero or nearly zero. This is correct for the material in which the spin configuration is C_1+C_3. However the material with the spin configuration C_2 vanishes when $\vec{H}=0$ and in such a case $\vec{H}_l$ must be regarded as a parameter to be chosen to fit the experimental data. Since $\vec{H}_l$ is independent of $\vec{H}$, while $\vec{H}_i$ depends on both the magnitude and orientation of $\vec{H}$, regarding $\vec{H}_l$ as a parameter does not destroy the validity of using NMR experiments to check the functional form of $\vec{H}_i$.

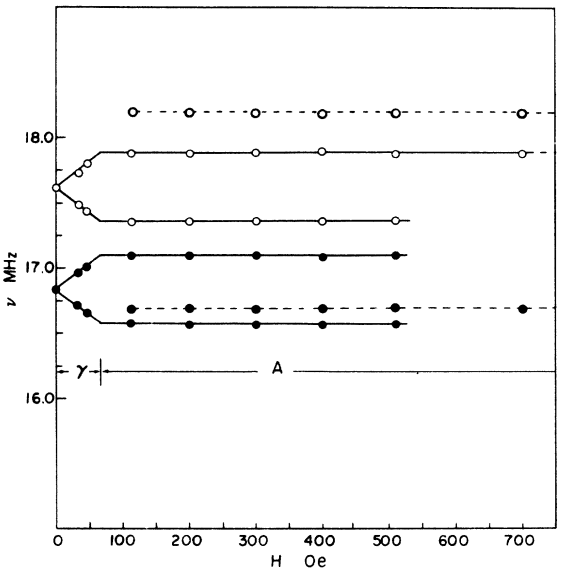

FIG. 7. Resonance frequencies of the water protons with H parallel to the c axis. Solid lines are resonances from material with a C_1+C_3 spin configuration. Dashed lines are resonances from material with a C_2 spin configuration. $T=2.25$°K.

We consider first the resonances from the water protons in the material for which the spin arrangement corresponds to $Pnm'a'$ (i.e., to the configuration C_1+C_3). The magnitude and direction of the local fields $\vec{H}_l$ at these sites is given in Table III. Each of the two nonequivalent local fields should occur in four different orientations to be consistent with $Pnm'a'$. However, the four vectors apparently lie so close to the xz plane that only two different orientations are distinguishable. The re-

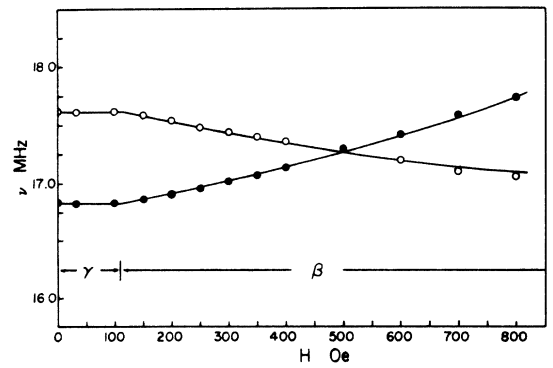

FIG. 8. Resonance frequencies of water protons with H parallel to the a axis. $T=2.25$°K.

sults obtained by applying an external field along the z axis ($\theta = 0$) are shown in Fig. 7. The two sets of lines originating from the zero-field resonances at 16.83 and 17.61 MHz belong to material with the $C_1 + C_3$ spin configuration. Resonances from the $C_1 + C_3$ configuration can be distinguished from those of C_2 by the fact that as H increases the $C_1 + C_3$ resonances *decrease* in intensity, while the C_2 resonances increase in intensity. The lines consisting only of dashes in Fig. 7 connect points belong to the C_2 configuration, which will be discussed later. The solid lines drawn through the experimental $C_1 + C_3$ points were obtained by inserting the values of H_{iz} from Eqs. (21b) and (17b) and data from Table III in Eq. (22).

If the external field is applied along the x axis ($\theta = 90°$) one obtains the results shown in Fig. 8. The curves drawn through the experimental points were calculated by inserting expressions for H_{ix} from Eqs. (21a) and (20a) and the data of Table III in Eq. (22). The value of H_a required in Eq. (20a) was read from the break in the curves at the junction between the γ and β regions. This gave $H_a = 111$ Oe. The correctness of the fit in the β region depends on the correctness of the value of ϑ given in Table III. Thus this experiment is an alternative method of determining ϑ.

Figure 9 shows the results of an experiment in which an external field of magnitude $H = 520$ Oe was applied at varying angles θ measured from the z axis. In such a case the crystal passes through the region A, B, and β, and expressions for H_{ix} and H_{iz} appropriate to these regions must

TABLE IV. Parameters of the internal field from experimental data.

$H_k = 64$ Oe
$H_a = 111$ Oe
$H_c = 790$ Oe
$r = M_a/M_c = 0.21$

be used in Eq. (22). The parameter $H_a = 111$ Oe was fixed by the results of the previous paragraph and the two remain parameters H_c and $r = M_a/M_c$ were chosen to fit the experimental data. The set of parameters required to fit $\vec{H}_i$ to the data shown in Figs. 7–9 are summarized in Table IV. Although these parameters were obtained by using only data on the water protons in the $C_1 + C_3$ materials they should be equally valid for other nuclei and in either $C_1 + C_3$ or C_2 material. For the protons in the $(CH_3)_3NH$ groups in $C_1 + C_3$ material, we have found this to be the case; since this situation gives no new information we turn to the water proton resonances which arise from C_2 material.

As previously noted, the frequency dependence of the C_2 water proton resonance for a field along z axis is given by the dashed lines of Fig. 7. The angle dependence of the frequencies of the water protons in C_2 material for $H = 520$ Oe is shown in Fig. 10. One notes that these resonances disappear in the β region, as required for C_2 material. In fitting the data on C_2 resonances shown in Fig. 7 and Fig. 10 one only has freedom to pick

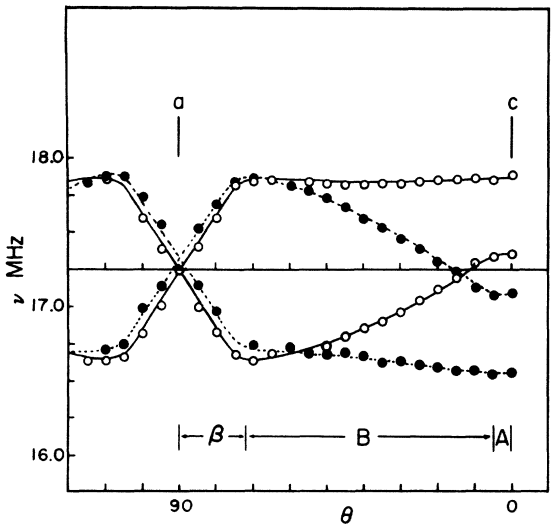

FIG. 9. Angular variation of the resonance frequencies of water protons in a field of 520 Oe. The resonances arise from material having the C_1 and C_3 spin configurations. $T = 2.25$ °K.

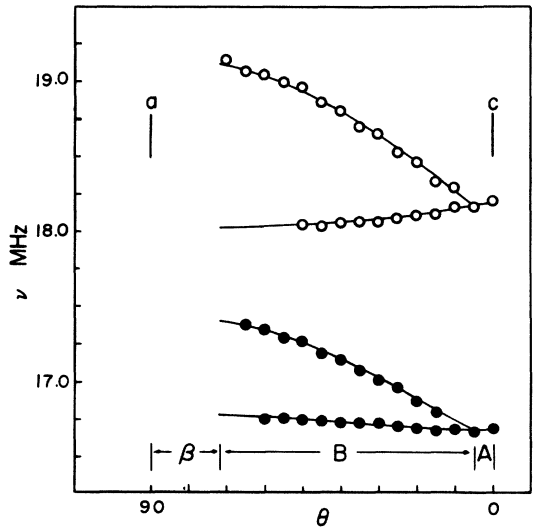

FIG. 10. Angular variation of resonance frequencies of water protons in material having the C_2 spin configuration in a field of 520 Oe. The C_2 configuration does not exist in the β region of the magnetization diagram. $T = 2.25$ °K.

TABLE V. Local fields for water protons in C_2 material.

Site	Magnitude[a] (kOe)	ϑ, angle from $+z$ axis
1, 2	4.211	$-20.0°$
3, 4	4.211	$+20.0°$
5, 6	3.854	$+11.5°$
7, 8	3.854	$-11.5°$

[a]At 2.25 °K.

the fixed local-field vectors $\vec{H}_l$, since the parameters which specify the behavior of $\vec{H}_i$ have been determined by the previous experiments. The $\vec{H}_l$ vectors which determine the curves drawn through the experimental C_2 points in these two figures are given in Table V. Comparing the $\vec{H}_l$ vectors given for $C_1 + C_3$ in Table III with those for C_2 in Table V, one notes that the magnitudes of the vectors are quite similar and the orientations are only modified as required by the difference in magnetic symmetry. This probably reflects the fact that the major contribution to the $\vec{H}_l$ arises from the dipolar field from the nearest Co moment.

The local fields at the chlorine sites in the chain are determined primarily by the transferred hyperfine interaction with the Co ions to which the Cl ions are bonded. As a result one expects the local magnetic fields to be of nearly the same magnitude, regardless of whether the spin configuration is $C_1 + C_3$ or C_2. Furthermore the local field $\vec{H}_l$ is expected to be large compared to $\vec{H}_i$, as long as the magnetization is unsaturated, and therefore $\vec{H}_i$ will produce only a small perturbation of the frequencies of each of the zero field transitions. The behavior of the 10.075 MHz transition in an applied field along the z axis is shown in Fig. 11. At fields just above 64 Oe the intensities of the two components are nearly the same and at such fields one interprets the components as arising from alternating $\vec{H}_l$ directions in adjacent bc planes of the $C_1 + C_3$ spin configuration. In the C_2 configuration the $\vec{H}_l$ directions should all be parallel to $\vec{H}_i$. Experimentally one observes that as $\vec{H}$ is increased the ratio of the intensity of the high-frequency component to the low-frequency component increases rapidly and the high-frequency component is observable long after the lower component has disappeared below noise level. Apparently the resonance from the C_2 material is superimposed on the high-frequency component of the resonance from the $C_1 + C_3$ material.

VI. FIELD AND ANGLE DEPENDENCE OF THE MAGNETIZATION

In Sec. V we have shown that a number of the parameters describing the magnetic behavior of $CoCl_3[(CH_3)_3NH] \cdot 2H_2O$ may be obtained from NMR results. Such parameters may also be determined by measuring the field dependence of the magnetization. As indicated in Sec. IV the parameters M_a, M_c, and H_k are independent of the shape of the crystal. In contrast the quantities H_a and H_c depend on the shape of the sample through the demagnetization factors.

Figure 12 shows the field dependence of M_x and M_z at $T = 2.09$ °K. By extrapolating the linear portions of the low- and high-field sections of the magnetization curves to intersections one finds

$$M_a = 12.0 \text{ emu/g} = 21.2 \text{ emu/cm}^3$$

and

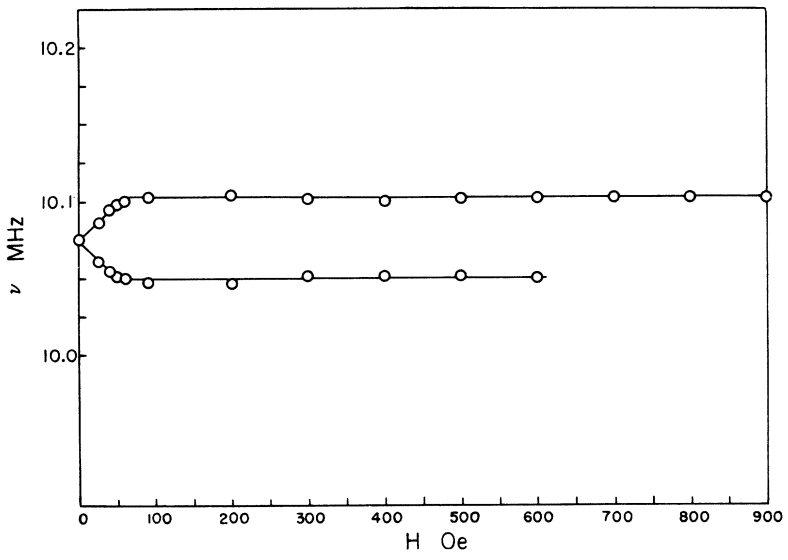

FIG. 11. Splitting of the 10.075 MHz Cl^{35} line in an applied field parallel to the c axis. $T = 2.5$ °K.

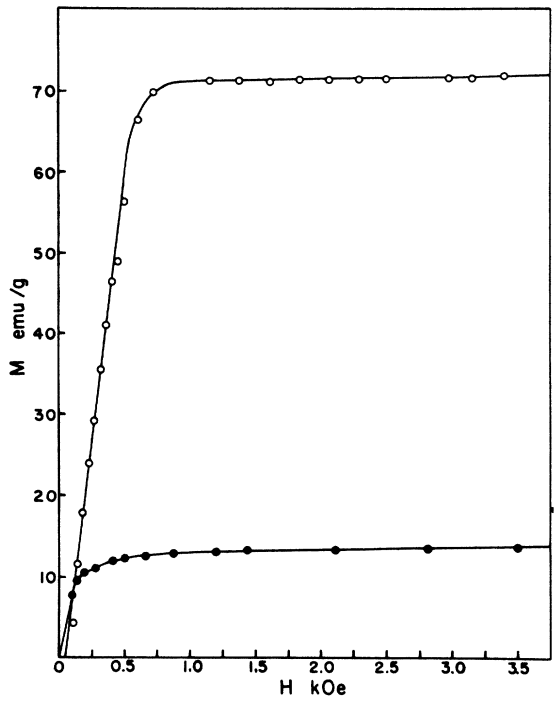

FIG. 12. Field dependence of M_x (solid circles) and M_z (open circles) at $T=2.09\,^\circ$K.

$$M_c = 71.0 \text{ emu/g} = 127.4 \text{ emu/cm}^3.$$

This yields the ratio $r = M_a/M_c = 0.17$, which may be compared to $r = 0.21$ obtained by fitting the NMR data. Let Θ be the angle of inclination of the moments with respect to the $\pm z$ axis in the C_1 and C_3 configuration or with respect to the $+z$ axis in the C_2 configuration, then

$$\tan\Theta = r \,. \tag{23}$$

From this expression one obtains, $\Theta = 12.1^\circ$ from the NMR experiments and $\Theta = 9.8^\circ$ from the magnetization experiments. Since the fit of the NMR data is rather insensitive to the exact value of r, we regard the value of Θ obtained from the magnetization data as the more accurate. One should be careful to note that the canting angle Θ is *not* the same as the angle ϑ given in Table III. The latter represents the inclination of the local field (at a nuclear site) with respect to the z axis. The fact that ϑ is approximately equal to Θ for the water protons merely reflects the fact that the direction of the Co^{++} moment is roughly parallel to the lines connecting the Co ion and the water protons.

If the applied field H is oriented at some angle other than $\theta = 0$ (the z axis) or $\theta = 90^\circ$ (the x axis) the magnetization parallel to H is given by

$$M_H = M_x \sin\theta + M_z \cos\theta \,. \tag{24}$$

Figure 13 shows the observed angle dependence of M_H for $H = 490$ Oe and $T = 2.1\,^\circ$K. The curve passing through the experimental points was fitted by inserting in Eq. (24) the appropriate expressions for M_x and M_z given in Sec. IV. The parameters used in fitting the data consisted of the values of M_a and M_c from the magnetization data and $H_k = 64$, $H_a = 250$, $H_c = 558$ Oe. The value of H_k was taken from NMR results and is considered more precise than the value $H_k \sim 60$ Oe obtained by extrapolating M_z to zero. The values of H_a and H_c were chosen to give the best fit to the experimental M_H data. The values of H_a and H_c so determined are in qualitative agreement with the fields at the intersection points of the linear portions of the low- and high-field sections of the M_x and M_z curves given in Fig. 12. The shapes of the crystals used in the NMR and magnetization experiments were quite different, and since H_a and H_c depend on the sample shape through the demagnetization factors one must expect these fields to be quite different in the two experiments. Comparing the values of H_a and H_c from the magnetization experiment with those from the NMR experiment given in Table IV shows that this is indeed the case. If the samples were *uniformly magnetized* and ellipsoidal in shape one should have[5,6]

$$\sum_i N_{ii} = 4\pi \,. \tag{25}$$

The samples used in the NMR experiments were approximately prolate spheroids elongated along the b axis and of axial ratio 1 : 3. Calculating N_{xx} and N_{zz} from the NMR values of H_a and H_c and computing N_{yy} from the axial ratio one finds

$$\sum_i N_{ii} = 12.7 \sim 4\pi \,,$$

even though the samples were certainly not uni-

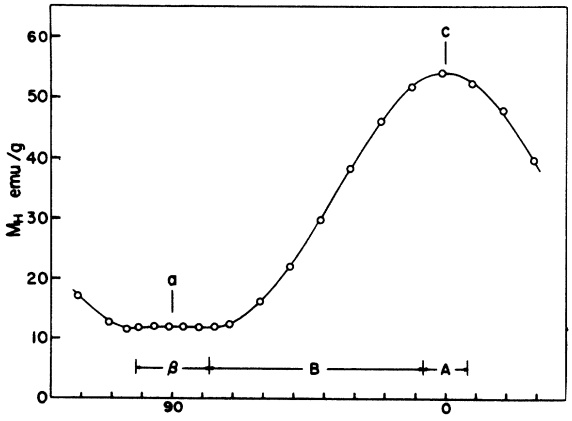

FIG. 13. Angular variation of M_H with $H = 490$ Oe. $T = 2.1\,^\circ$K.

formly magnetized at $H = 520$ Oe. For the samples used in the magnetization experiments the corresponding number is $\sum_i N_{ii} \sim 17$. The difference between the two situations probably stems from the fact that the crystals used in the magnetization experiments were used "as grown," with no attempt to shape them in ellipsoidal form.

The success of the simple theory (Sec. IV) in predicting the form of the angular variation of the NMR frequencies and the magnetization, must be considered as indicating that this theory is essentially correct. At the same time it must be recognized that there are certain defficiencies in the development given in Sec. IV. Since the expressions relating the magnetization and internal fields are derived by minimizing the energy, the results are invalid in nonequilibrium situations. For example one observes that the magnetization is slightly different depending on whether the applied field H is increasing or decreasing. Furthermore, this difference increases as the temperature is reduced. It is likely that such hysteresis arises from nonequilibrium magnetization distributions in the neighborhood of imperfections in the crystals.

Probably an even more serious objection to the development given in Sec. IV lies in the fact that we have assumed that the spin configurations C_1, C_2, C_3 are undistorted by the applied field. The gradual increase in M_x for $H > H_a$ and in M_z for $H > H_c$ shown in Fig. 12 demonstrates that such an assumption in only an approximation.

ACKNOWLEDGMENTS

The authors wish to thank Professor J. A. Cowen of Michigan State University and Dr. W. J. M. de Jonge of the Eindhoven University of Technology for their continued interest and aid in this work. Special thanks are extended to J. L. Knirk for aid in collecting the NMR data and to P. Koomen and P. Uiterhoeven for aid in collecting magnetization data. The authors gratefully acknowledge support by the National Science Foundation (R.D.S.) and "Stichting voor Fundementeel Onderzoek der Materie" and "Nederlandse Organisatie voor Zuiver Wetenschappelijk Onderzoek" (A.C.B.).

---

[1]D. B. Losee, J. N. McElearney, G. E. Shankle, R. N. Carlin, P. J. Cresswell, and Ward T. Robinson, Phys. Rev. B 8, 2185 (1973).

[2]W. Opechowski and R. Guccione, in *Magnetism*, edited by G. T. Rado and H. Suhl (Academic, New York, 1965), Vol. 2A, Chap. 3.

[3]Apparently a corresponding situation exists in the canted antiferromagnet $FeCl_2 \cdot 4H_2O$. See R. D. Spence, R. Au, and P. A. van Dalen, Physica 30, 1612 (1964).

[4]The methods used here are similar to those used to discuss spin-flop domains in MnF_2. See A. R. King and D. Paquette, Phys. Rev. Lett. 30, 662 (1973).

[5]J. A. Osborn, Phys. Rev. 67, 351 (1945).

[6]E. Schlöman, J. Appl. Phys. 33, 2825 (1962).